

¹ Supplementary Materials File

² Alejandro Damian-Serrano, Steven H.D. Haddock, Casey W. Dunn

³ Supplementary Methods

⁴ DAPC optimization: Some taxa have inapplicable states for certain absent characters (such as
⁵ the length of a nematocyst subtype that is not present in a species), which are problematic for
⁶ DAPC analyses. We tackled this by transforming the absent states to zeroes. This approach
⁷ allows us to incorporate all the data, but creates an attraction bias between small character
⁸ states (*e.g.* small tentilla) and absent states (*e.g.* no tentilla). Absent characters are likely to
⁹ be very biologically relevant to prey capture and we believe they should be accounted for
¹⁰ in a predictive approach. We limited the number of linear discriminant functions retained
¹¹ to the number of groupings in each case. We selected the number of principal components
¹² retained using the a-score optimization function (R adegenet::optim.a.score) (Jombart et
¹³ al. 2010) with 100 iterations, which yielded more stable results than the cross validation
¹⁴ function (R adegenet::xval). This optimization aims to find the compromise value with
¹⁵ highest discrimination power with the least overfitting.

¹⁶ Supplementary Materials

¹⁷ Other trees inferred in this work include:

¹⁸ The constrained tree inferences utilized the following constrain topology:

2.1) Definitions of homologous structures used throughout this work.

| Structure | Definition |
|-------------------|--|
| Haploneme | Nematocyst with no shaft |
| Heteroneme | Nematocyst with a distinct shaft |
| Desmoneme | Small oval/tapered adhesive nematocyst with thick coiled tubule |
| Rhopaloneme | Small rod-like nematocyst found on the terminal filament |
| Terminal filament | Distal extension of the tentillum beyond the cnidoband |
| Cnidoband | Distinct packing of nematocysts on the dorsal side of the tentillum |
| Tentacle | Tubular projection from the gastrozooid basigaster |
| Tentillum | Evenly spaced dorsal evagination of the tentacle carrying ordered and functional nematocysts |
| Involucrum | Extension of the pedicle covering part of the cnidoband |
| Pedicle | Proximal region of the tentillum between the cnidoband and the tentacle |
| Elastic strand | Mesoglea derived collagenous double strand underlying the cnidoband of some siphonophores |

2.2) Definitions of the continuous morphological and kinematic characters measured.

| Character | Definition | Units |
|--------------------------------------|---|---------------------|
| Cnidoband length | Distance from the base to the tip of the cnidoband in natural position | micrometers |
| Cnidoband free length | Distance from the base to the tip of the cnidoband when stretched straight | micrometers |
| Cnidoband width | Diameter of the cnidoband on the widest point | micrometers |
| Involucrum length | Length of the involucrum from the base of the cnidoband to its most distal extent | micrometers |
| Heteroneme length | Length of the heteronemes | micrometers |
| Heteroneme width | Diameter of the heteronemes at the widest point | micrometers |
| Heteroneme shaft length | Length of the heteroneme shaft | micrometers |
| Heteroneme shaft width | Width of the heteroneme shaft | micrometers |
| Heteroneme number | Number of heteronemes in each tentillum (# in each row*2) | micrometers |
| Haploneme length | Length of the haplonemes | micrometers |
| Haploneme width | Diameter of the haplonemes at the widest point | micrometers |
| Rhopaloneme length | Length of the rhopalonemes | micrometers |
| Rhopaloneme width | Diameter of the rhopalonemes at the widest point | micrometers |
| Desmoneme length | Length of the desmonemes | micrometers |
| Desmoneme width | Diameter of the cnidoband at the widest point | micrometers |
| Involucrum length | Length of the involucrum from the base of the cnidoband to its most distal extent | micrometers |
| Elastic strand width | Diameter of the descending elastic strand at the widest point | micrometers |
| Pedicle width | Diameter of the pedicle | micrometers |
| Tentacle width | Diameter of the tentacle | micrometers |
| Haploneme row number | Number of haploneme rows running parallel to the length of the cnidoband | micrometers |
| Cnidoband coiledness | Cnidoband free length / Cnidoband length | adimensional |
| Heteroneme elongation | Heteroneme Length/Width | adimensional |
| Haploneme elongation | Haploneme Length/Width | adimensional |
| Desmoneme elongation | Desmoneme Length/Width | adimensional |
| Rhopaloneme elongation | Rhopaloneme Length/Width | adimensional |
| Heteroneme shaft extension | Heteroneme shaft length / Heteroneme capsule length | adimensional |
| Nematocyst Surface area | $4\pi^2((L\text{Length}^2)/(\text{Width}^2))^1.6 \times ((\text{Width}/2)^2)^1.6)/(3)^{1/1.6}$ | micrometers squared |
| Nematocyst volume | Ellipsoid formula : $(4/3)\pi^1(L\text{Length}^2)(\text{Width}^2)^2$ | micrometers cubed |
| Nematocyst SA/V ratio | Nematocyst surface area / Nematocyst volume | 1/micrometers |
| Total haploneme volume | Haploneme volume * Haploneme row number * (Cnidoband free length / Haploneme width) | micrometers cubed |
| Total heteroneme volume | Heteroneme volume * Heteroneme number | micrometers cubed |
| Total nematocyst volume | Total haploneme volume + Total heteroneme volume | micrometers cubed |
| Total discharge time | Time from initial cnidoband movement to complete conformational change | milliseconds |
| Average CB discharge speed | Distance covered by the leading edge of the discharging cnidoband in the total discharge time. | mm/s |
| Maximum CB discharge speed | Maximum speed attained by the leading edge of the discharging cnidoband | mm/s |
| Heteroneme discharge speed AVG | Distance covered by the heteroneme nematocyst tubule from initial ejection to full eversion in the time it takes to evert fully | mm/s |
| Heteroneme discharge free speed AVG | Distance covered by the heteroneme nematocyst tubule in the time it takes to evert fully, accounting for coiling. | mm/s |
| Heteroneme discharge speed MAX | Maximum speed attained by the non-shaft tubule of the heteroneme nematocysts during eversion. | mm/s |
| Heteroneme discharge free speed MAX | Maximum speed attained by the non-shaft tube of the heteroneme nematocysts during eversion, accounting for coiling. | mm/s |
| Heteroneme shaft discharge speed MAX | Maximum speed attained by the shaft of the tubule of the heteroneme nematocysts during initial eversion. | mm/s |
| Heteroneme filament length | Distance covered by the heteroneme nematocyst tubule from initial ejection to full eversion | micrometers |
| Haploneme discharge speed AVG | Distance covered by the haploneme nematocyst tubule from initial ejection to full eversion in the time it takes to evert fully. | mm/s |

Figure 1: Character definitions.

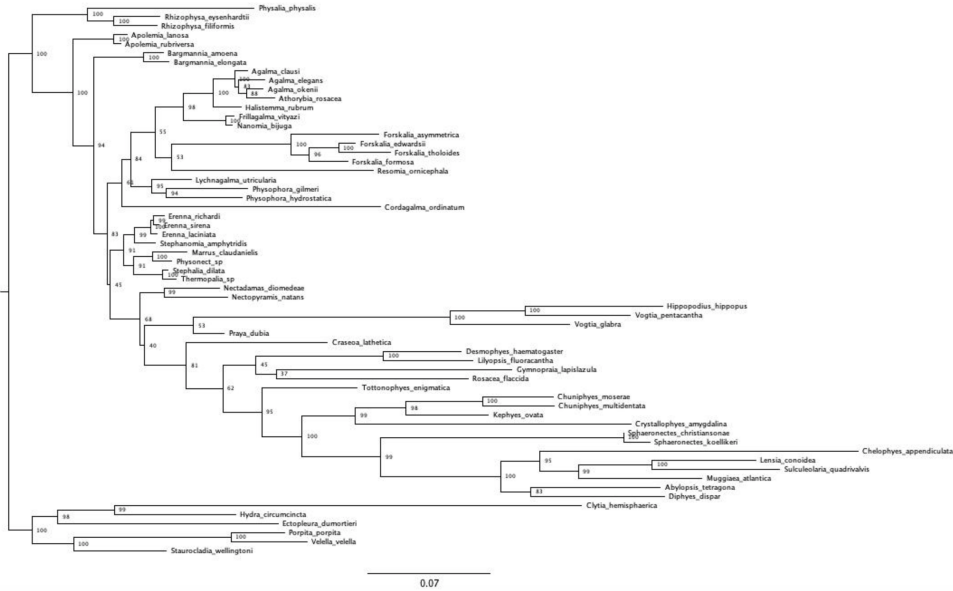


Figure 2: Maximum likelihood IQTree inference, unconstrained. Node labels are bootstrap support values.

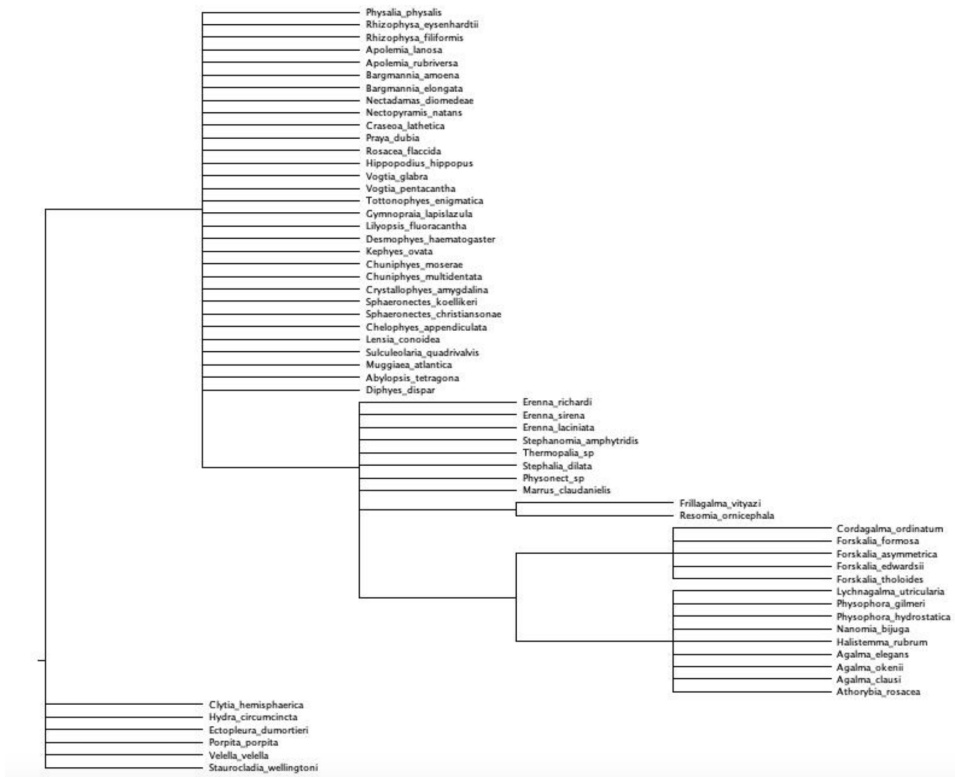


Figure 3: Topology used to constrain analyses (minimal topological statements based on the incongruences between the unconstrained tree and Munro et al. (2018)).

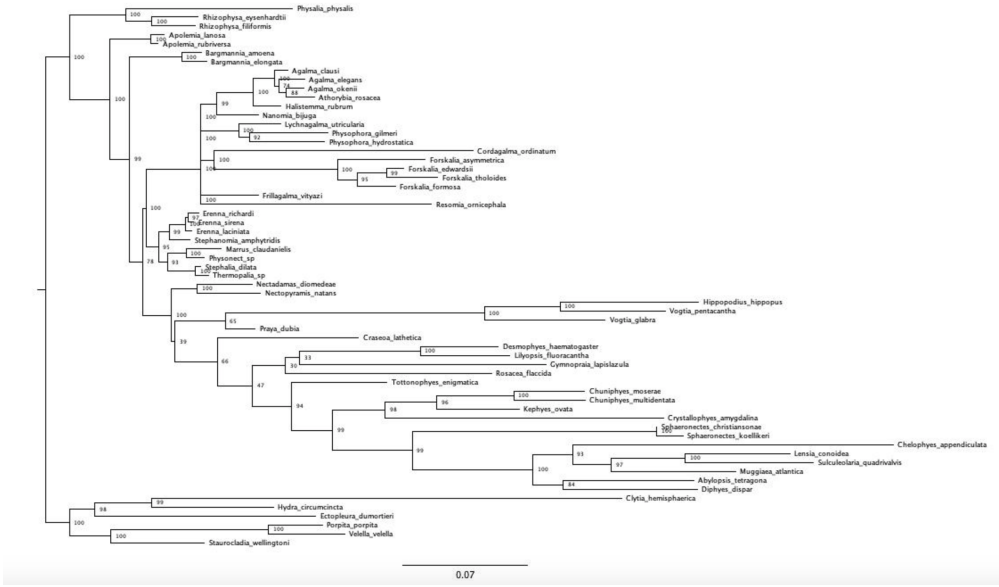


Figure 4: Constrained IQTree ML inference. Node labels are bootstrap support values.

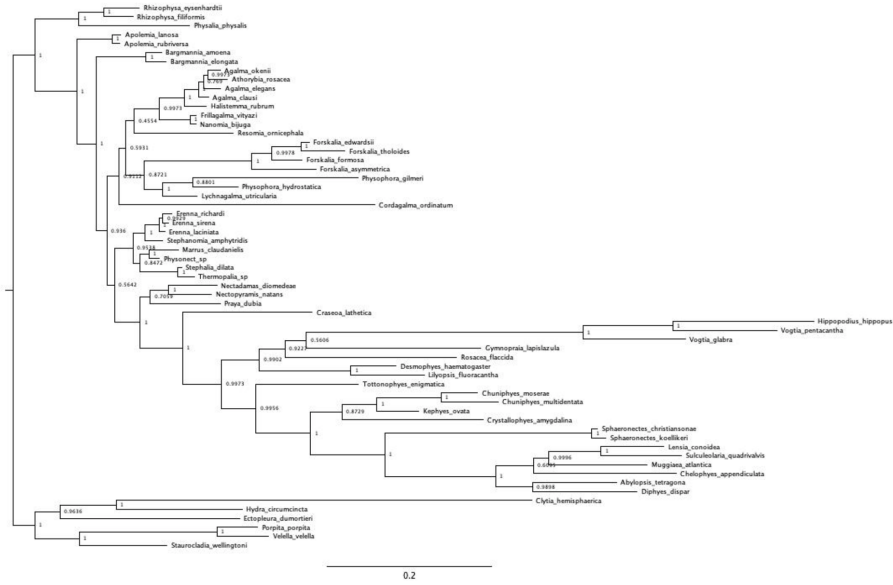


Figure 5: Unconstrained Bayesian topology inference in RevBayes (node labels are Bayesian posteriors).

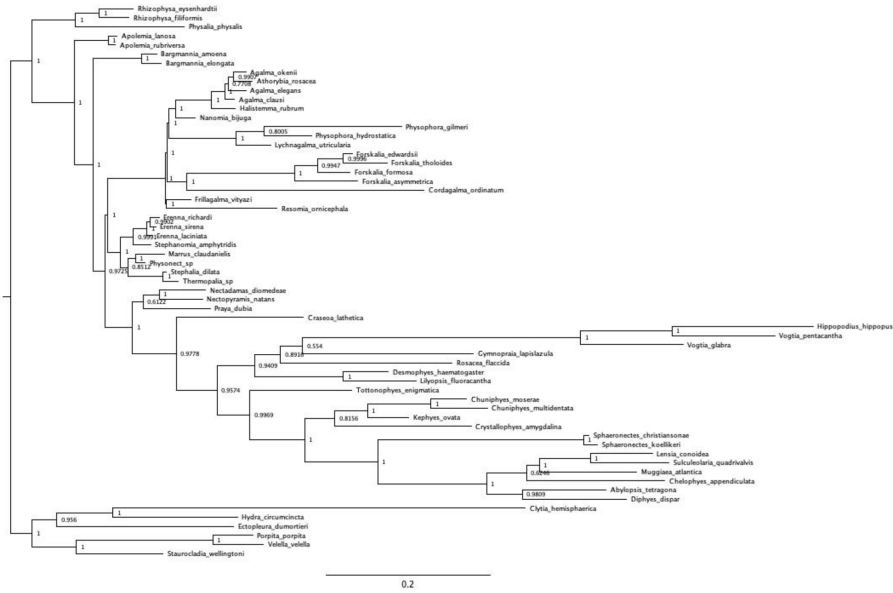


Figure 6: Clade constrained Bayesian inference in RevBayes (node labels are Bayesian posteriors).

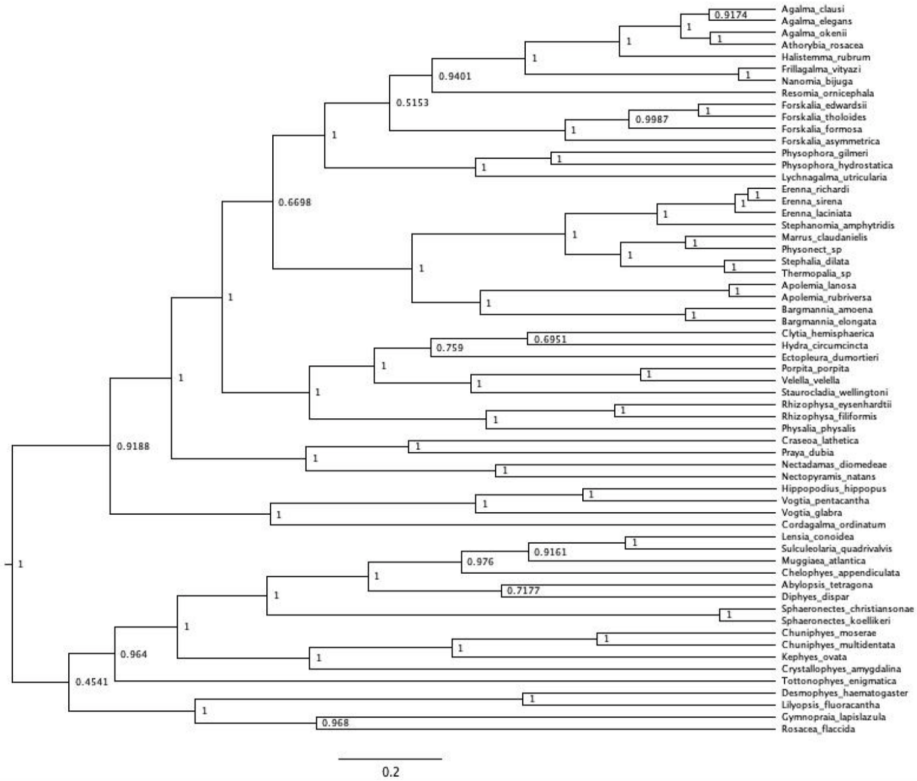


Figure 7: Unconstrained ultrametric Bayesian time tree branch length and topology inference in RevBayes (node labels are Bayesian posteriors). Arbitrary rooting.).

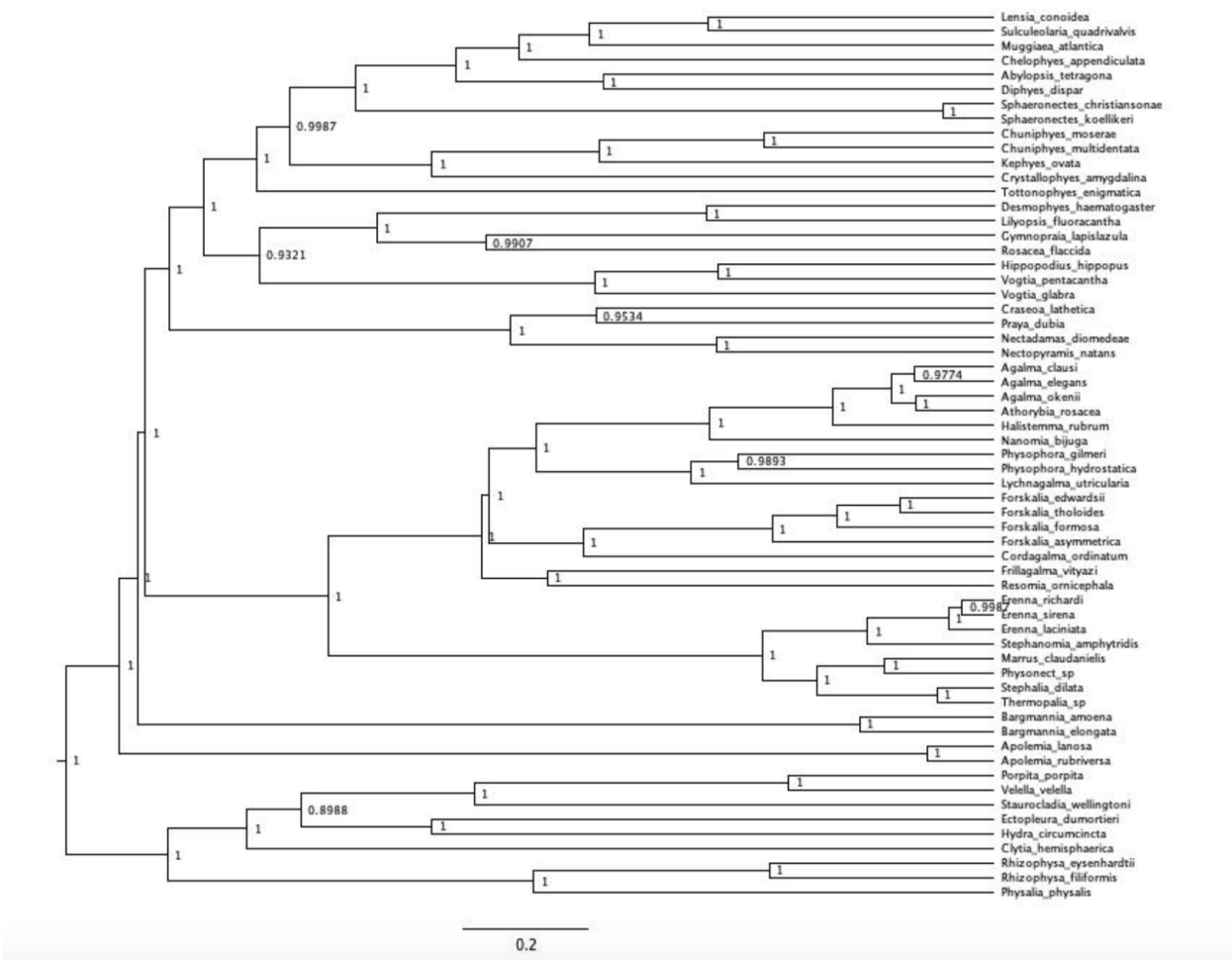


Figure 8: Ultrametric Bayesian time tree branch length inference in RevBayes (node labels are bayesian posteriors). Topology clamped to the Bayesian constrained topology inference in @ref{Bayes_constrained}. Tree rooted using outgroup constraint.

¹⁹ DAPC discriminant analyses:

| Character | Non-Phylogenetic dAIC | BM dAIC | EB dAIC | OU dAIC | K | K p-value | Ntaxa |
|--|-----------------------|---------|---------|---------|-------|-----------|-------|
| Haploneme elongation | 0 | 2.017 | 4.332 | 2.38 | 0.583 | 0.001 | 43 |
| Desmoneme elongation | 0 | 3.232 | 5.693 | 3.183 | 0.018 | 0.864 | 31 |
| Heteroneme shaft width μm | 0 | 5.346 | 7.67 | 2.581 | 0.45 | 0.005 | 42 |
| Elastic strand width μm | 0 | 1526 | 3.938 | 1.296 | 0.706 | 0.001 | 34 |
| Desmoneme length μm | 0.518 | 0 | 2.46 | 0.578 | 0.566 | 0.002 | 31 |
| Heteroneme shaft extension | 0.589 | 0 | 2.324 | 1.965 | 0.041 | 0.970 | 42 |
| Haploneme SA/V | 0.91 | 0 | 2.315 | 2.291 | 0.156 | 0.132 | 43 |
| Total heteroneme volume μm^3 | 0.961 | 0 | 2.352 | 2.328 | 0.248 | 0.046 | 39 |
| Rhopaloneme width μm | 1.205 | 0 | 2.46 | 1.321 | 0.308 | 0.123 | 31 |
| Heteroneme volume μm^3 | 2.002 | 0 | 2.153 | 2.324 | 0.196 | 0.117 | 42 |
| Involucrum length μm | 2.479 | 0 | 2.498 | 2.492 | 0.529 | 0.001 | 29 |
| Tentacle width μm | 2.939 | 0 | 2.307 | 1.974 | 0.367 | 0.044 | 44 |
| Cnidoband coiledness | 3.077 | 0 | 2.315 | 1.786 | 0.174 | 0.043 | 43 |
| Total haploneme volume μm^3 | 3.641 | 0 | 1.852 | 2.296 | 0.198 | 0.267 | 43 |
| Cnidoband free length μm | 3.801 | 0 | 2.132 | 2.315 | 0.325 | 0.007 | 43 |
| Heteroneme free length μm | 3.82 | 0 | 2.01 | 1.325 | 0.301 | 0.080 | 42 |
| Rhopaloneme elongation | 3.852 | 0 | 2.145 | 2.46 | 0.062 | 0.827 | 31 |
| Desmoneme width μm | 3.96 | 0 | 2.46 | 2.121 | 0.553 | 0.004 | 31 |
| Cnidoband length μm | 4.094 | 0 | 1.911 | 2.315 | 0.321 | 0.015 | 43 |
| Heteroneme number | 4.262 | 0 | 2.352 | 2.219 | 0.866 | 0.001 | 39 |
| Heteroneme shaft free length μm | 4.553 | 0 | 2.324 | 2.321 | 0.331 | 0.126 | 42 |
| Rhopaloneme length μm | 5.599 | 0 | 2.46 | 2.457 | 0.589 | 0.001 | 31 |
| Heteroneme/Cnidoband length | 5.671 | 0 | 1.862 | 2.342 | 1.068 | 0.001 | 42 |
| Pedicle width μm | 6.566 | 0 | 2.253 | 2.315 | 0.541 | 0.001 | 43 |
| Haploneme width μm | 7.495 | 0 | 2.218 | 2.304 | 0.553 | 0.001 | 43 |
| Heteroneme width μm | 7.53 | 0 | 2.324 | 1.647 | 0.502 | 0.001 | 42 |
| Heteroneme elongation | 14.169 | 0 | 0.819 | 2.23 | 0.508 | 0.001 | 42 |
| Haploneme row number | 19.566 | 0 | 2.114 | 2.315 | 0.442 | 0.001 | 43 |
| Total nematocyst volume μm^3 | 21.007 | 0 | 2.213 | 2.292 | 1.3 | 0.001 | 45 |
| Cnidoband width μm | 5.69 | 0.307 | 0 | 2.623 | 0.374 | 0.001 | 43 |
| Haploneme free length μm | 12.337 | 7.125 | 0 | 9.439 | 1.079 | 0.001 | 43 |

Non-phylogenetic model supported

Brownian Motion model supported

Early Burst model supported

Figure 9: Model support (delta AICc), phylogenetic signal (Blomberg's K), and phylogenetic signal permutation test p-value for each continuous character. Ntaxa = Number of taxa used in the analyses after removing those where the character state is inapplicable or the data is missing.

| Variable | Best model | Msig | Cvar | Svar | Sasr | Shgt | Dcfid |
|--|------------|-------|-------|-------|-------|-------|-------|
| Desmoneme length μm | WN | 0.889 | 0.224 | 0.084 | 0.32 | 0.146 | 0 |
| Heteroneme shaft extension | WN | 0.861 | 0 | 0.577 | 0 | 0.533 | 0.042 |
| Total heteroneme volume | WN | 0.895 | 0.577 | 0.006 | 0.026 | 0.078 | 0.603 |
| Rhopaloneme width μm | WN | 0.823 | 0.42 | 0.182 | 0.014 | 0.531 | 0.006 |
| Haploneme free length μm | EB | 0.841 | 0.052 | 0.036 | 0.168 | 0.226 | 0.843 |
| Heteroneme volume μm^3 | BM | 0.855 | 0.731 | 0.228 | 0.897 | 0.775 | 0.104 |
| Involucrum length μm | BM | 0.839 | 0.01 | 0.018 | 0.116 | 0.09 | 0.987 |
| Tentacle width μm | BM | 0.817 | 0.841 | 0.402 | 0.386 | 0.785 | 0.48 |
| Cnidoband coiledness | BM | 0.873 | 0 | 0.028 | 0.016 | 0.144 | 0.41 |
| Total haploneme volume | BM | 0.807 | 0.228 | 0.004 | 0.006 | 0.024 | 0.398 |
| Cnidoband free length μm | BM | 0.825 | 0.076 | 0.002 | 0 | 0.006 | 0.681 |
| Heteroneme free length μm | BM | 0.859 | 0.392 | 0.386 | 0.056 | 0.591 | 0.284 |
| Rhopaloneme elongation | BM | 0.873 | 0.022 | 0.006 | 0.004 | 0.048 | 0.104 |
| Desmoneme width μm | BM | 0.813 | 0.877 | 0.531 | 0.014 | 0.941 | 0.014 |
| Cnidoband length μm | BM | 0.829 | 0.096 | 0 | 0 | 0.004 | 0.901 |
| Heteroneme number | BM | 0.823 | 0.312 | 0 | 0.004 | 0.02 | 0.869 |
| Heteroneme shaft free length μm | BM | 0.877 | 0.468 | 0.565 | 0.034 | 0.841 | 0.851 |
| Rhopaloneme length μm | BM | 0.829 | 0.525 | 0.547 | 0.01 | 0.917 | 0.08 |
| Heteroneme/cnidoband length | BM | 0.839 | 0.01 | 0 | 0.004 | 0.008 | 0.715 |
| Cnidoband width μm | BM | 0.907 | 0.977 | 0 | 0.002 | 0.01 | 0.11 |
| Pedicle width μm | BM | 0.817 | 0.931 | 0.476 | 0.088 | 0.969 | 0.813 |
| Haploneme width μm | BM | 0.881 | 0.805 | 0.12 | 0.294 | 0.511 | 0.15 |
| Heteroneme width μm | BM | 0.849 | 0.142 | 0.156 | 0.356 | 0.819 | 0.278 |
| Heteroneme elongation | BM | 0.933 | 0.094 | 0.07 | 0.681 | 0.791 | 0.777 |
| Haploneme row number | BM | 0.863 | 0 | 0.002 | 0.004 | 0.008 | 0.012 |

Figure 10: Model adequacy scores for the best model supported for each morphological character. Cvar = coefficient of variation of the absolute value of the contrasts. Svar = Slope of a linear model fitted to the absolute value of the contrasts against their expected variances. Sasr = slope of the contrasts against the ancestral state inferred at each corresponding node. Shgt = slope of the contrasts against node depth. Dcfid = Kolmogorov-Smirnov D-statistic comparing contrasts to a normal distribution with SD equal to the root of the mean of squared contrasts.

| Character | N | dAICc BM | dAICc OU1 | dAICc OUm | Msig | Cvar | Svar | Sasr | Shgt | Dcfid | |
|--|----|----------|-----------|-----------|-------|-------|-------|-------|-------|-------|-------|
| Haploneme elongation | 21 | 0 | 0.953 | 713.671 | 0.801 | 0 | 0.038 | 0.156 | 0.362 | 0.098 | |
| Heteroneme shaft width μm | 19 | 0 | 1.051 | 632.503 | 0.767 | 0.801 | 0.128 | 0.092 | 0.4 | 0.813 | |
| Cnidoband width μm | 21 | 0 | 1.595 | 761.241 | 0.781 | 0.723 | 0.072 | 0.09 | 0.31 | 0.228 | |
| Heteroneme shaft free length μm | 19 | 0 | 1.649 | 628.334 | 0.791 | 0.402 | 0.941 | 0.098 | 0.575 | 0.464 | |
| Heteroneme volume μm^3 | 19 | 0 | 2.105 | 629.21 | 0.779 | 0.034 | 0.39 | 0.338 | 0.637 | 0.392 | |
| Haploneme width μm | 21 | 0 | 2.452 | 766.546 | 0.779 | 0.599 | 0.316 | 0.791 | 0.995 | 0.288 | |
| Pedicle width μm | 21 | 0 | 2.458 | 764.406 | 0.815 | 0.791 | 0.368 | 0.26 | 0.963 | 0.298 | |
| Heteroneme width μm | 19 | 0 | 2.516 | 634.229 | 0.805 | 0.809 | 0.292 | 0.208 | 0.709 | 0.38 | |
| Tentacle width μm | 22 | 0 | 2.702 | 383.12 | 0.835 | 0.496 | 0.344 | 0.867 | 0.096 | 0.444 | |
| Heteroneme to CB | 19 | 0 | 0.127 | NA | | 0.811 | 0.336 | 0.004 | 0.068 | 0.026 | 0.434 |
| Haploneme surface area:volume | 21 | 0 | 2.282 | 757.267 | 0.747 | 0.563 | 0.392 | 0.583 | 0.927 | 0.15 | |
| Heteroneme elongation | 19 | 0.217 | 0 | 618.621 | 0.819 | 0.601 | 0.012 | 0.707 | 0.062 | 0.715 | |
| Total nematocyst volume | 22 | 0.57 | 0 | 378.872 | 0.809 | 0.501 | 0.06 | 0.088 | 0.266 | 0.501 | |
| Heteroneme free length μm | 19 | 0.746 | 0 | 627.372 | 0.811 | 0.885 | 0.593 | 0.156 | 0.368 | 0.679 | |
| Total haploneme volume | 21 | 1.281 | 0 | 730.592 | 0.829 | 0.452 | 0.038 | 0.134 | 0.096 | 0.819 | |
| Cnidoband length μm | 21 | 1.439 | 0 | 763.478 | 0.761 | 0.328 | 0.04 | 0.11 | 0.098 | 0.803 | |
| Cnidoband free length μm | 21 | 2.219 | 0 | 760.518 | 0.843 | 0.35 | 0.012 | 0.066 | 0.05 | 0.911 | |
| Cnidoband coiledness | 21 | 2.669 | 0 | 765.921 | 0.807 | 0.002 | 0.008 | 0.03 | 0.076 | 0.791 | |
| Haploneme row number | 21 | 4.177 | 0 | 729.95 | 0.825 | 0.004 | 0.002 | 0.06 | 0.006 | 0.346 | |
| Haploneme free length μm | 21 | 5.497 | 0 | 778.011 | 0.793 | 0.388 | 0.032 | 0 | 0.052 | 0.306 | |
| Heteroneme shaft extension | 19 | 6.17 | 0 | 611.533 | 0.775 | 0 | 0.068 | 0.665 | 0.124 | 0.184 | |
| Rhopaloneme elongation | 13 | 144.229 | 146.783 | 0 | 0.753 | 0.641 | 0.434 | 0.188 | 0.933 | 0.617 | |
| Desmoneme length μm | 13 | 148.14 | 151.403 | 0 | 0.763 | 0.182 | 0.607 | 0.31 | 0.745 | 0.014 | |
| Rhopaloneme length μm | 13 | 150.731 | 154.198 | 0 | 0.739 | 0.803 | 0.24 | 0.03 | 0.14 | 0.316 | |
| Rhopaloneme width μm | 13 | 150.82 | 154.287 | 0 | 0.743 | 0.462 | 0.306 | 0.07 | 0.182 | 0.092 | |
| Desmoneme elongation | 13 | 159.594 | 158.584 | 0 | 0.719 | 0.206 | 0.074 | 0.094 | 0.036 | 0.993 | |
| Desmoneme width μm | 13 | 164.639 | 168.106 | 0 | 0.773 | 0.11 | 0.885 | 0.098 | 0.605 | 0.002 | |
| Involucrum length μm | 14 | 148.672 | 151.078 | 0 | 0.779 | 0.126 | 0.17 | 0.25 | 0.418 | 0.671 | |
| Elastic strand width μm | 15 | 473.984 | 477.156 | 0 | 0.827 | 0.921 | 0.184 | 0.064 | 0.953 | 0.785 | |
| Total heteroneme volume | 17 | 619.03 | 619.932 | 0 | 0.797 | 0.803 | 0.078 | 0.172 | 0.35 | 0.697 | |
| Heteroneme number | 17 | 620.836 | 620.193 | 0 | 0.777 | 0.39 | 0.008 | 0.074 | 0.056 | 0.054 | |

Brownian Motion Supported

Single Optimum OU Supported

Multiple Optima OU Supported

Figure 11: Model support (delta AICc) for each morphological character analyzed on the feeding guild reconstruction regime tree. OU1 = Single-optimum Ornstein-Uhlenbeck. OUm = Multi-optima Ornstein-Uhlenbeck. Model adequacy scores calculated for the best supported model only. Msig = mean of squared contrasts. Cvar = coefficient of variation of the absolute value of the contrasts. Svar = Slope of a linear model fitted to the absolute value of the contrasts against their expected variances. Sasr = slope of the contrasts against the ancestral state inferred at each corresponding node. Shgt = slope of the contrasts against node depth. Dcfid = Kolmogorov-Smirnov D-statistic comparing contrasts to a normal distribution with SD equal to the root of the mean of squared contrasts.

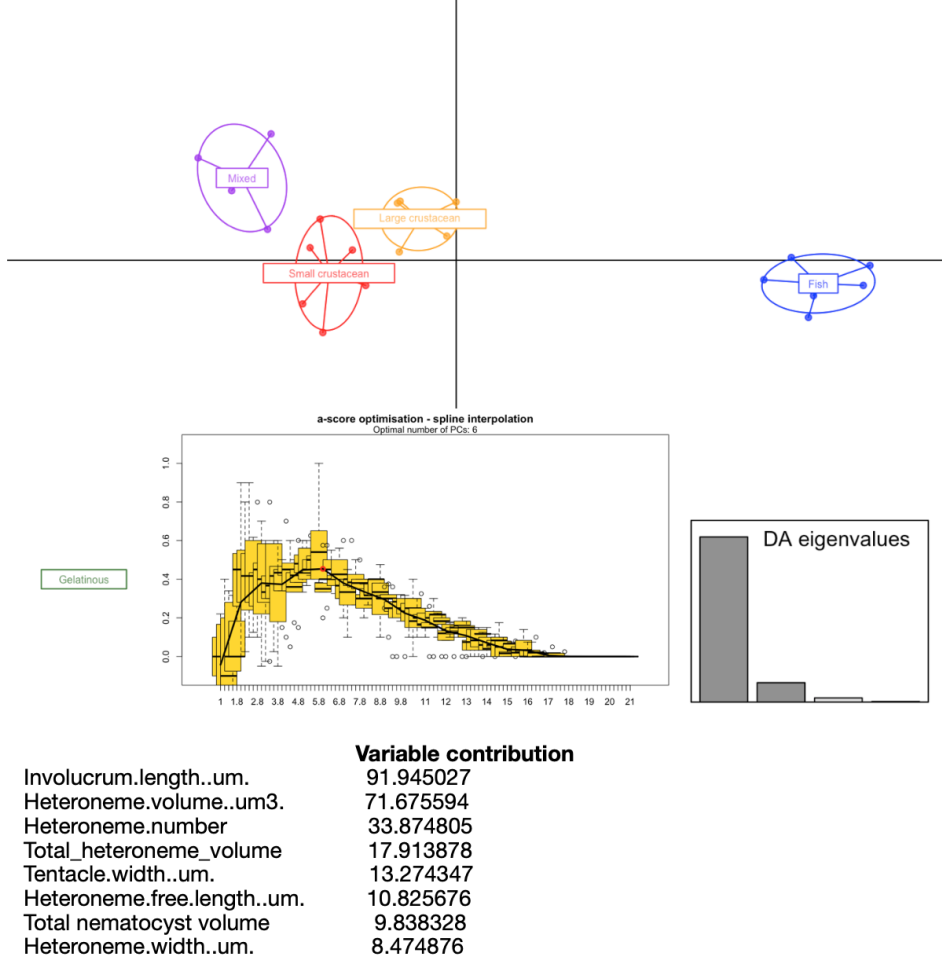
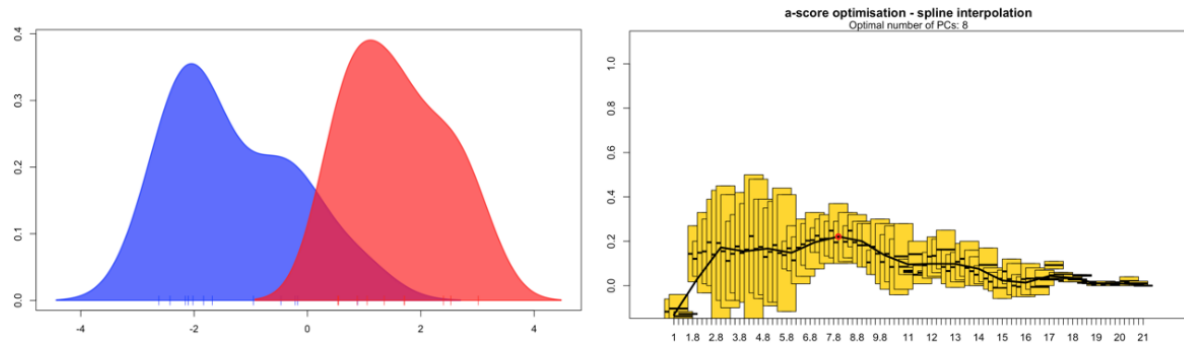


Figure 12: DAPC for Feeding guilds. Six PCs retained after a-score optimization (100 iterations). Four LDA functions used. Discriminant power on training set: 100%. Prediction posterior distribution heat map in main text Figure 6. Variable contribution (top quartile) calculated by the sum of the LDA variable loadings weighted by the eigenvalue of each LDA.



Variable contribution

| | |
|----------------------------|-----------|
| Total_nematocyst_volume | 12.810953 |
| Tentacle.width..um. | 5.687086 |
| haploneme_elongation | 4.586386 |
| SAV_haploneme | 4.264843 |
| Haploneme.row.number..um. | 2.966009 |
| Cnidoband.length..um. | 1.959479 |
| Cnidoband.width..um. | 1.679753 |
| Cnidoband.free.length..um. | 1.468262 |

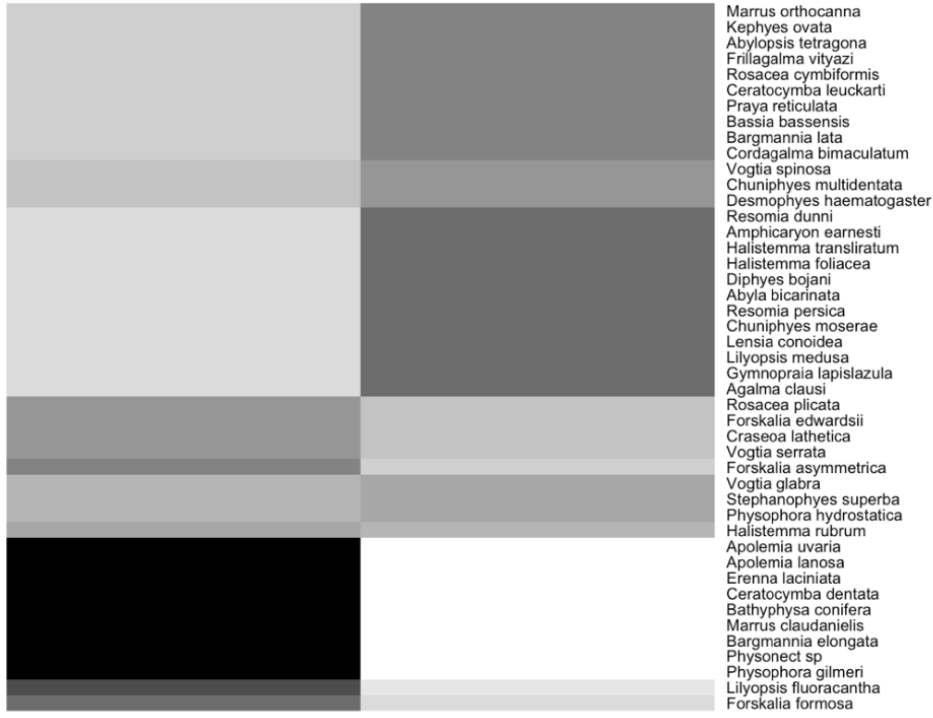
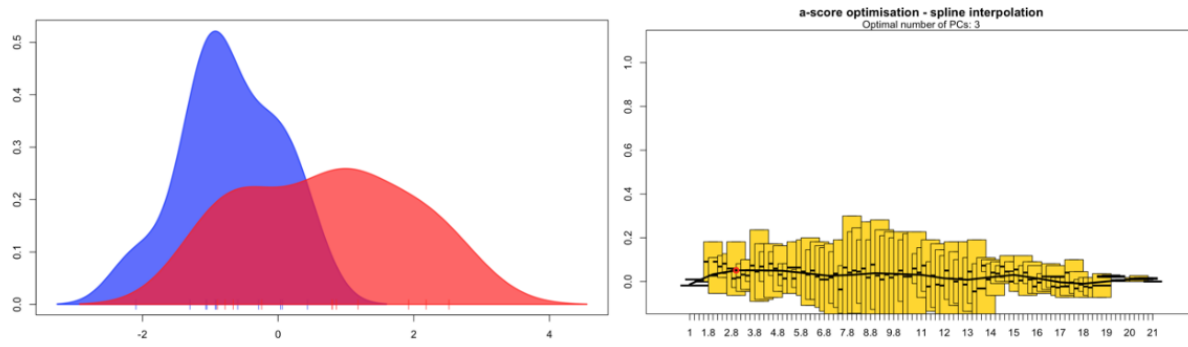


Figure 13: DAPC for copepod presence in the diet. Eight PCs retained after a-score optimization (100 iterations). One LDA functions used. Discriminant power on training set: 95.4%. Grayscale heat map shows the posterior probability distribution of the predictions. Variable contribution (top quartile) calculated by the sum of the LDA variable loadings weighted by the eigenvalue of each LDA.



Variable contribution

| | |
|----------------------------|-----------|
| total_haploneme_volume | 2.2734508 |
| Heteroneme.volume..um3. | 1.1308252 |
| total_nematocyst_volume | 1.1104459 |
| total_heteroneme_volume | 0.9402038 |
| Cnidoband.length..um. | 0.7583124 |
| Cnidoband.free.length..um. | 0.6650068 |
| Involucrum.length..um. | 0.6097537 |
| Pedicle.width..um. | 0.5447312 |

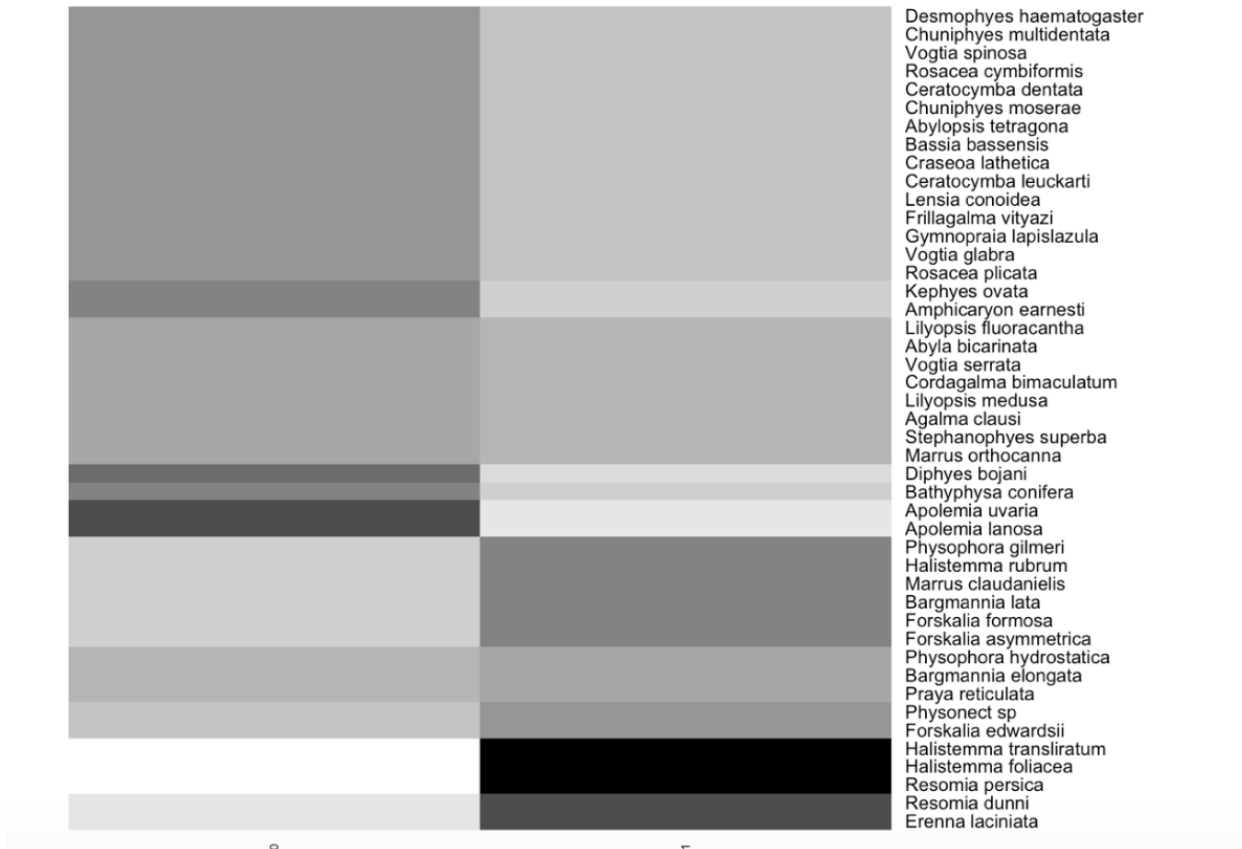
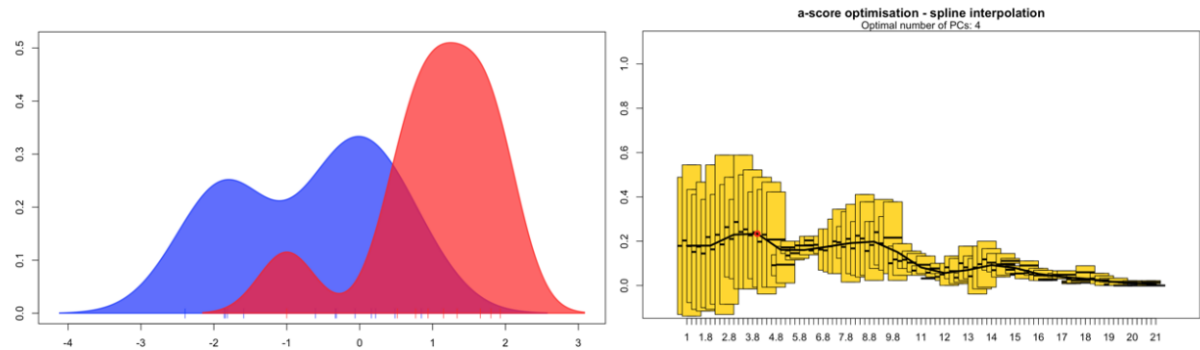


Figure 14: DAPC for fish presence in the diet. Three PCs retained after a-score optimization (100 iterations). One LDA function used. Discriminant power on training set: 68.1%. Grayscale heat map shows the posterior probability distribution of the predictions. Variable contribution (top quartile) calculated by the sum of the LDA variable loadings weighted by the eigenvalue of each LDA.



Variable contribution

| | Variable contribution |
|---------------------------|-----------------------|
| Involucrum.length..um. | 8.4739326 |
| total_heteroneme_volume | 2.0479062 |
| Elastic.strand.width..um. | 1.2640038 |
| Rhopaloneme.length..um. | 0.4274179 |
| Heteroneme.volume..um3 | 0.4255758 |
| haploneme_elongation | 0.3530771 |
| Desmoneme.length..um. | 0.3274451 |
| Tentacle.width..um. | 0.2763979 |

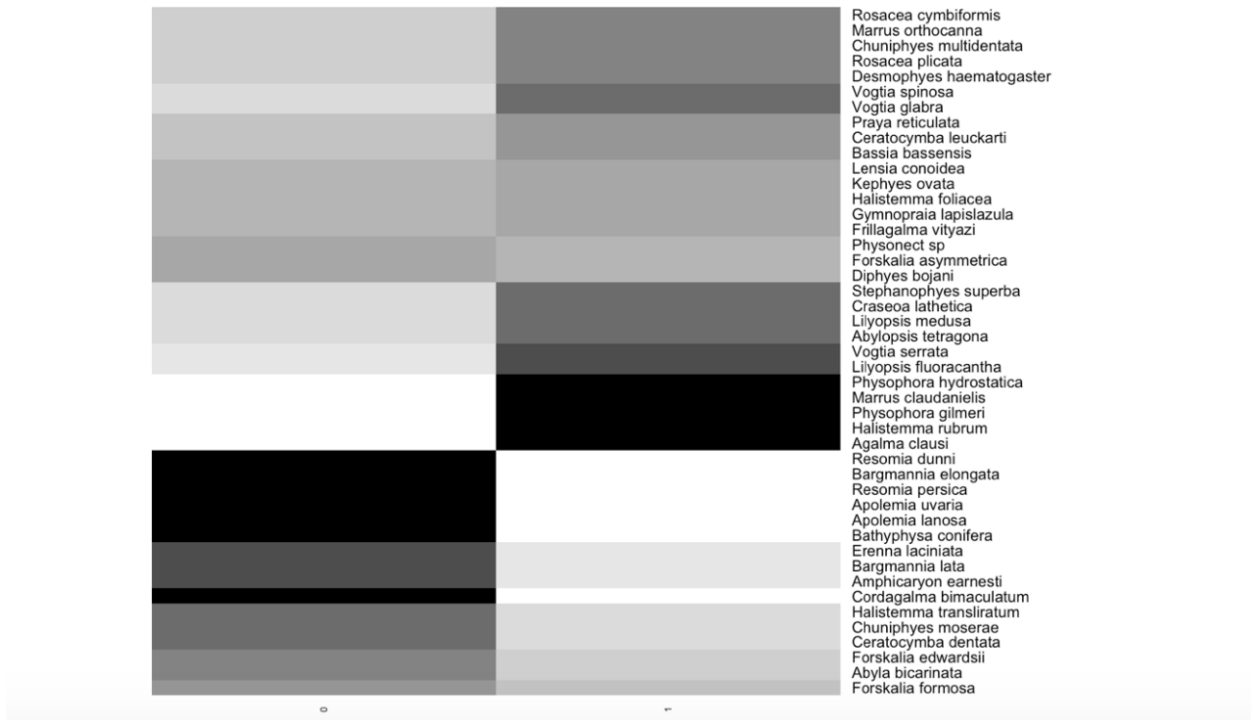


Figure 15: DAPC for large crustacean presence in the diet. Four PCs retained after a-score optimization (100 iterations). One LDA function used. Discriminant power on training set: 81.8%. Grayscale heat map shows the posterior probability distribution of the predictions. Variable contribution (top quartile) calculated by the sum of the LDA variable loadings weighted by the eigenvalue of each LDA.

| Character | Prey type | Ntaxa | phyloGLM AIC | phyloGLM P | phyloglm b | GLM AIC | GLM P | GLM b |
|--|---------------|-------|--------------|------------|------------|---------|-------|--------|
| Cnidoband coiledness | Decapod diet | 21 | 23.701 | 0.029 | 2.327 | 21.762 | 0.016 | 3.227 |
| Haploneme surface area:volume | Copepod diet | 21 | 19.143 | 0.017 | 3.246 | 17.355 | 0.017 | 4.631 |
| Haploneme width μm | Copepod diet | 21 | 18.844 | 0.017 | -3.098 | 16.997 | 0.019 | -4.417 |
| Pedicle width μm | Copepod diet | 21 | 22.182 | 0.032 | -1.16 | 23.723 | 0.024 | -1.437 |
| Tentacle width μm | Copepod diet | 22 | 22.038 | 0.026 | -1.543 | 23.634 | 0.025 | -1.505 |
| Cnidoband length μm | Copepod diet | 21 | 23.431 | 0.042 | -0.864 | 24.178 | 0.025 | -1.131 |
| Cnidoband width μm | Copepod diet | 21 | 22.887 | 0.035 | -1.545 | 23.658 | 0.027 | -1.89 |
| Heteroneme number | Copepod diet | 17 | 20.52 | 0.059 | -0.718 | 19.615 | 0.03 | -0.973 |
| Total haploneme volume | Copepod diet | 21 | 23.507 | 0.03 | -0.581 | 25.232 | 0.031 | -0.578 |
| Total heteroneme volume | Copepod diet | 17 | 17.156 | 0.032 | -0.533 | 16.369 | 0.031 | -0.758 |
| Pedicle width μm | Ostracod diet | 21 | 17.523 | 0.041 | -1.43 | 15.165 | 0.035 | -1.97 |
| Heteroneme shaft free length μm | Copepod diet | 19 | 23.955 | 0.076 | -1.53 | 23.378 | 0.04 | -2.16 |
| Haploneme width μm | Fish diet | 21 | 28.118 | 0.091 | 1.268 | 27.551 | 0.043 | 1.642 |
| Tentacle width μm | Fish diet | 22 | 28.927 | 0.058 | 0.804 | 28.771 | 0.044 | 0.874 |
| Haploneme surface area:volume | Fish diet | 21 | 28.258 | 0.098 | -1.329 | 27.596 | 0.044 | -1.768 |
| Total haploneme volume | Ostracod diet | 21 | 20.028 | 0.043 | -0.619 | 17.733 | 0.046 | -0.681 |
| Heteroneme volume μm^3 | Copepod diet | 19 | 24.282 | 0.091 | -0.521 | 24.297 | 0.046 | -0.72 |
| Pedicle width μm | Fish diet | 21 | 28.21 | 0.074 | 0.815 | 27.839 | 0.049 | 0.918 |

Figure 16: Logistic regressions between continuous morphological characters and prey type presences. Ntaxa = number of taxa used in the analyses after removing taxa with missing diet data and inapplicable character states. phyloGLM = Phylogenetic generalized logistic regression model. GLM = Generalized logistic regression model. P = p-value. b = slope. Only cases with significant GLM fits were retained. Cells colored blue indicate phyloGLM p-value < 0.05. Cells colored green indicate GLM p-value < 0.05

20 Ordinary and phylogenetic logistic regression of morphological characters and the pres-
 21 ence/absence of prey types:

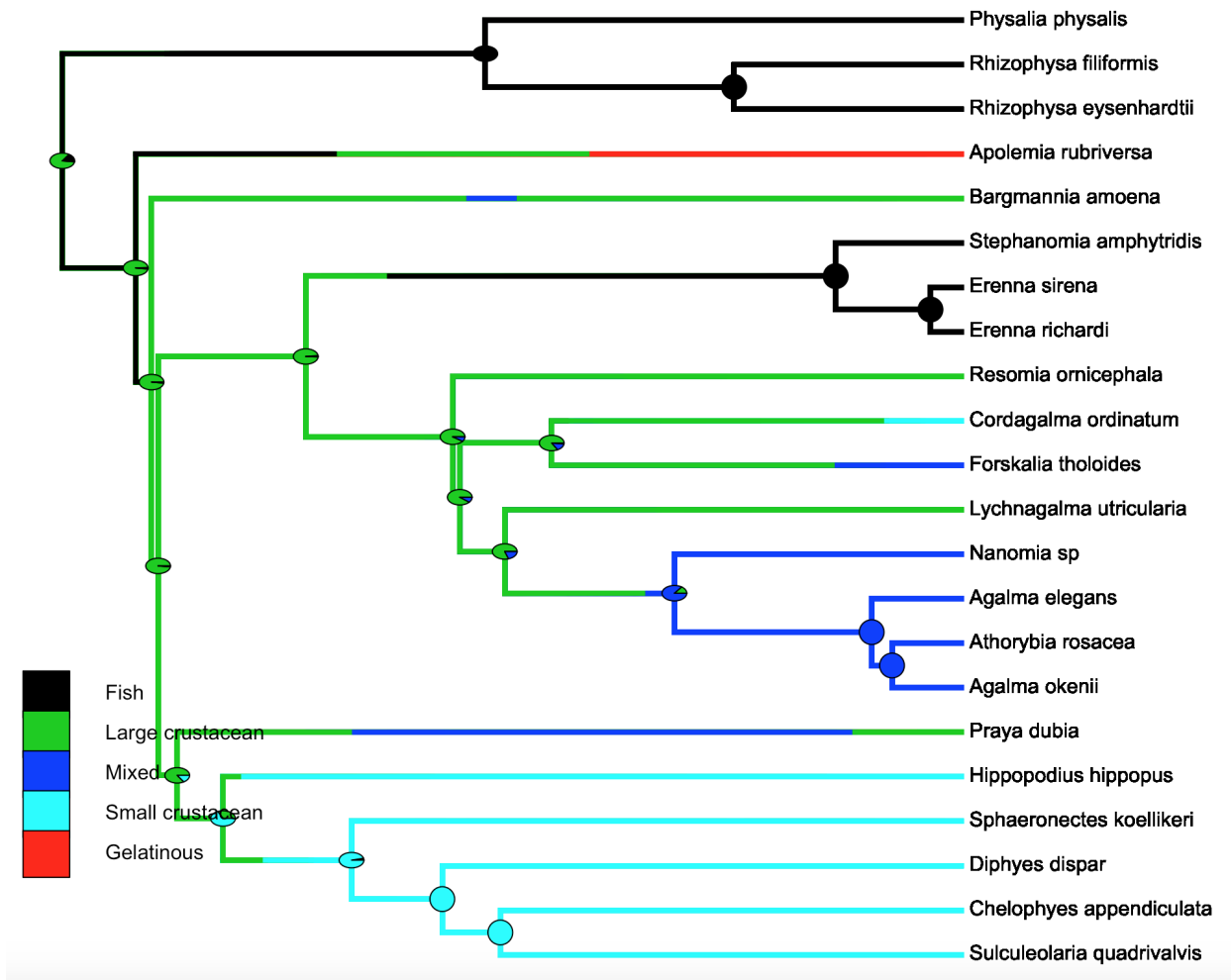


Figure 17: SIMMAP Feeding guilds.

²² Variance-Covariance Matrix analyses of phenotypic intergation and evolutionary modular-
²³ ity:

²⁴ **References**

²⁵ Jombart T., Devillard S., Balloux F. 2010. Discriminant analysis of principal components: A
²⁶ new method for the analysis of genetically structured populations. BMC genetics. 11:94.

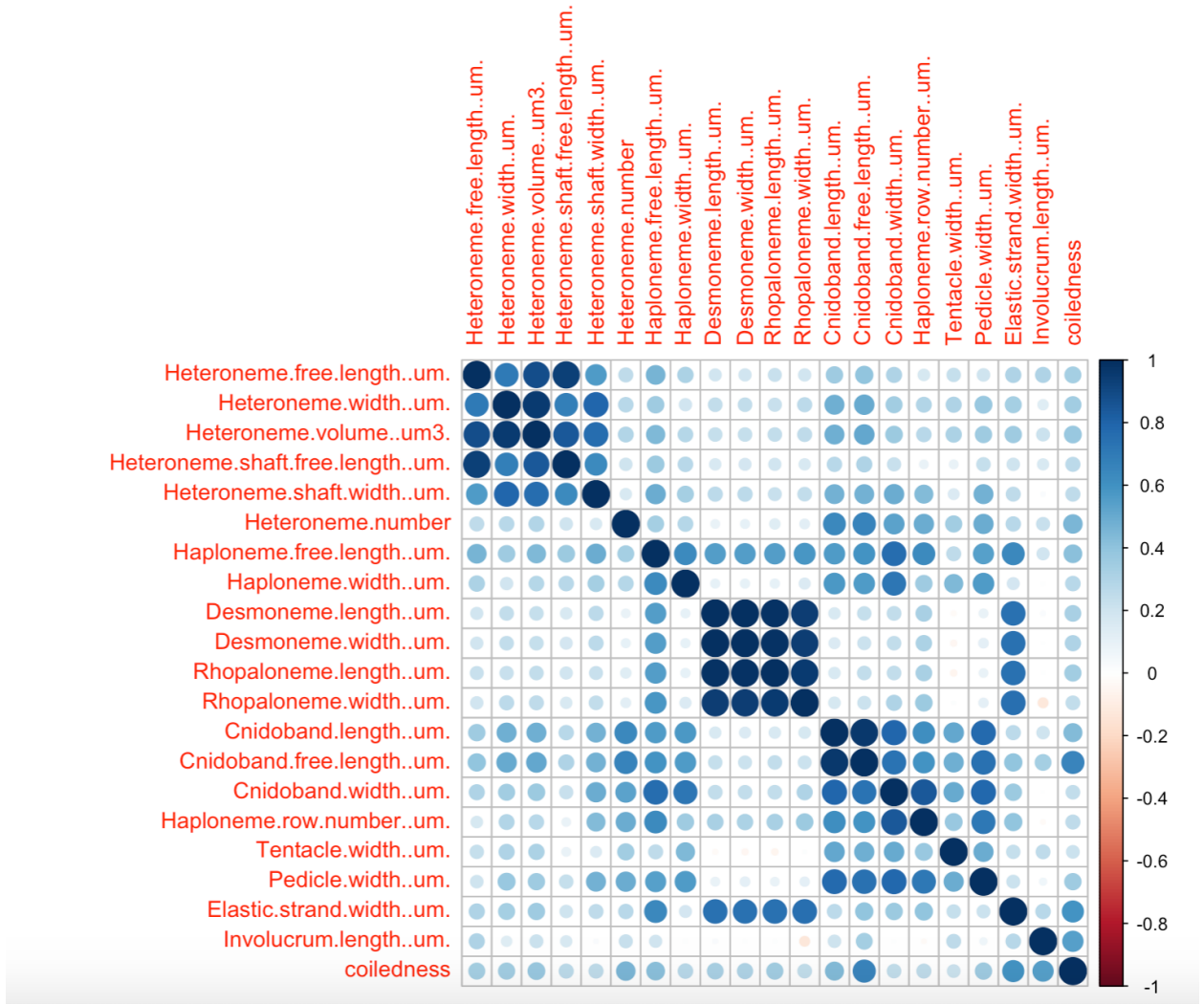


Figure 18: Rate covariance matrix for the whole tree using all taxa (45 species), transforming inapplicable states to zeroes. Covariances scaled to correlations. All characters estimated simultaneously under Brownian Motion.

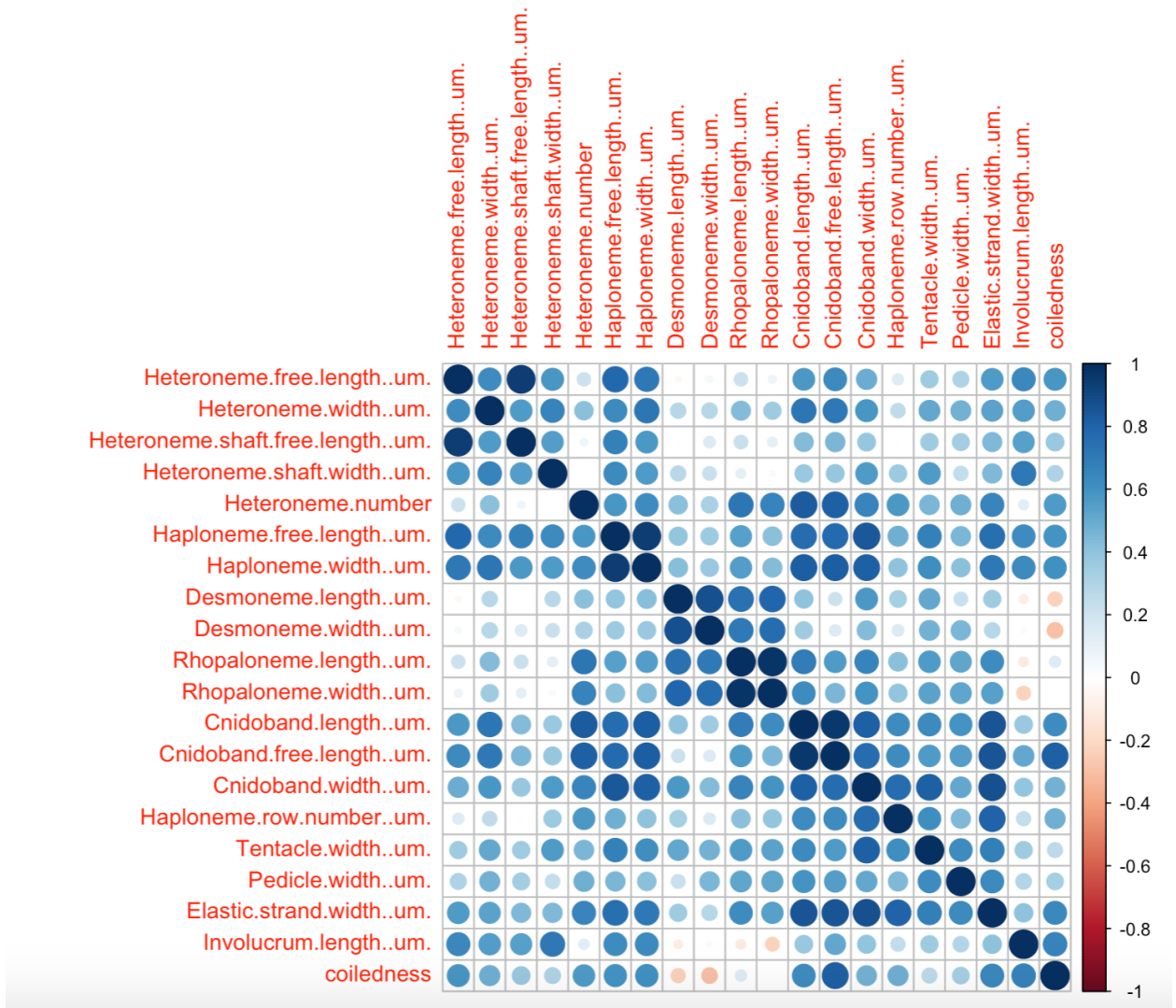


Figure 19: Rate covariance matrix for the whole tree using only taxa without inapplicable states (24 species). Covariances scaled to correlations. All characters estimated simultaneously under Brownian Motion.

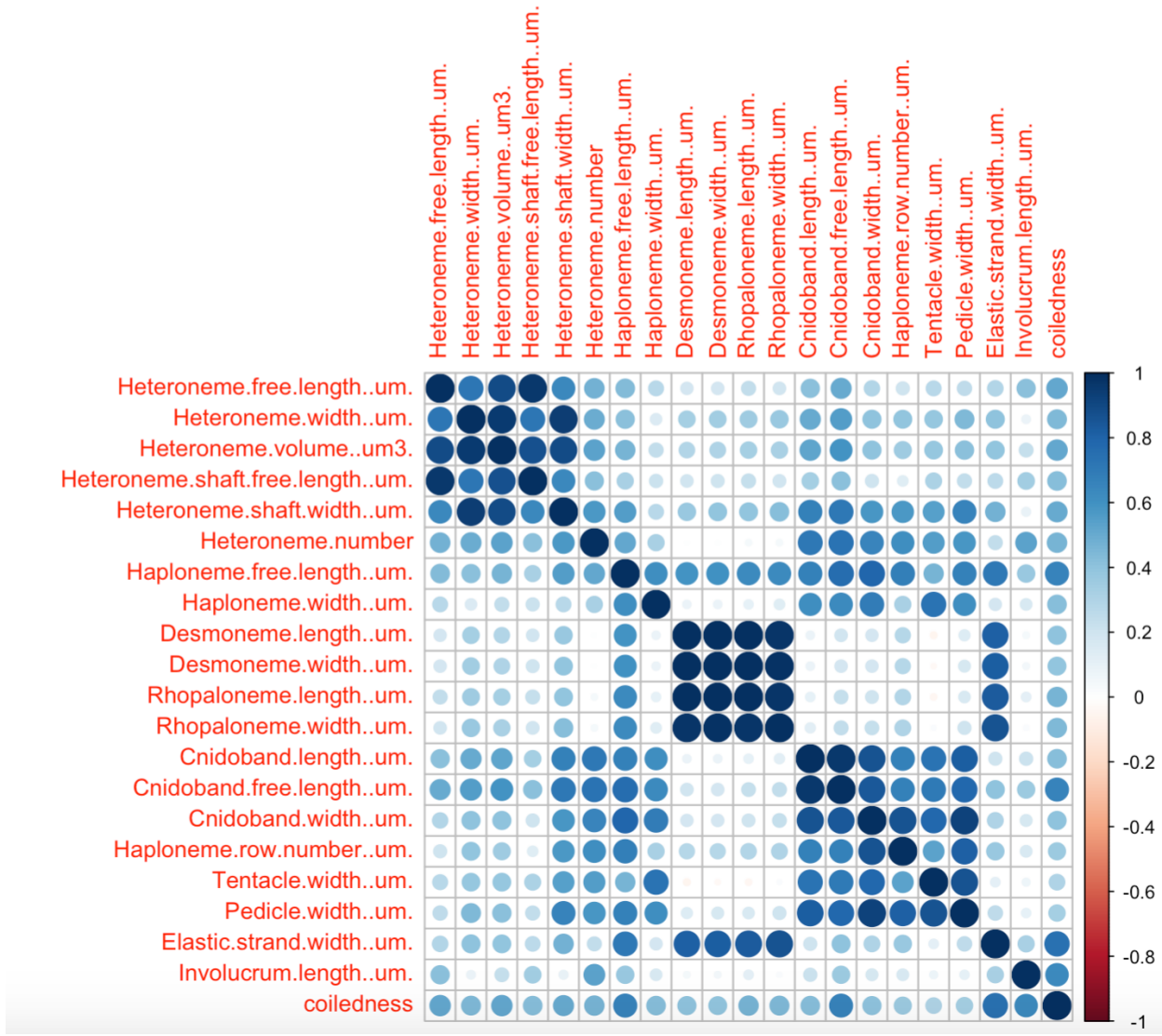


Figure 20: Rate covariance matrix for the whole tree using only taxa with diet data (22 species), transforming inapplicable states to zeroes. Covariances scaled to correlations. All characters estimated simultaneously under Brownian Motion.

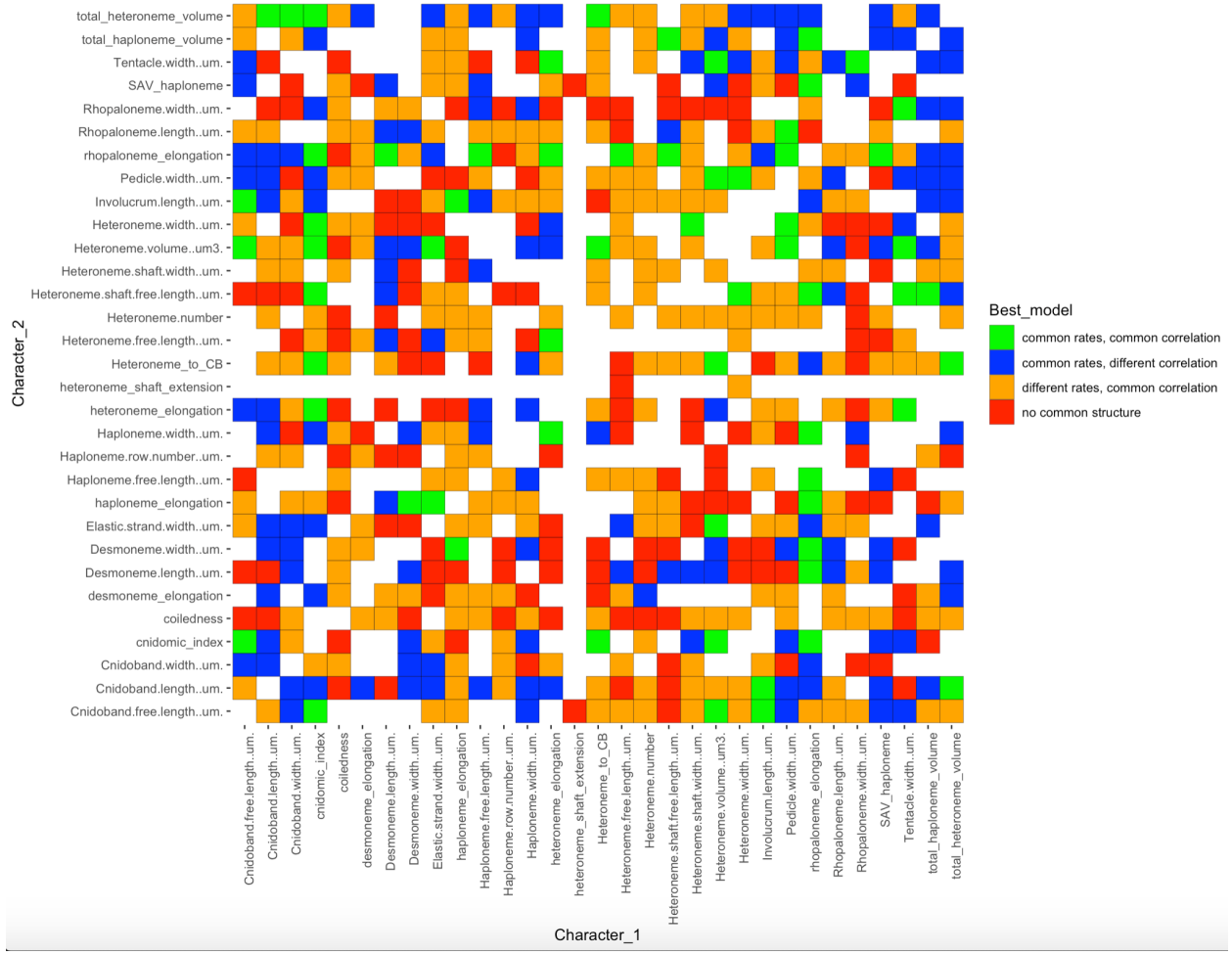


Figure 21: Best models (lowest AIC) supported in a pairwise character rate covariance analysis comparing correlated Brownian Motion models across the five selective regimes. Selective regimes were mapped onto the tree using an ancestral state reconstruction of the feeding guilds. Blank cells represent computationally singular contrasts.

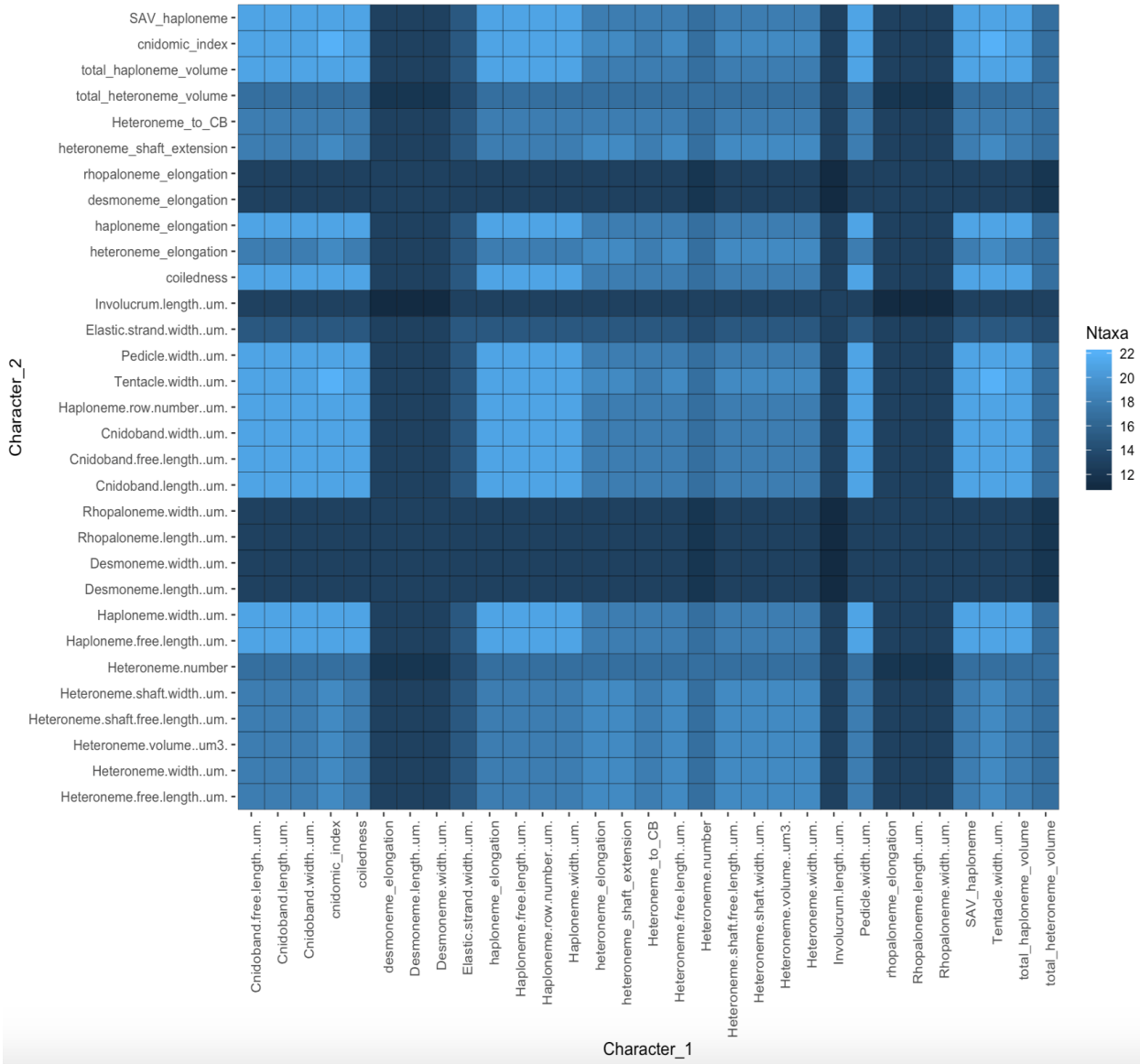


Figure 22: Number of taxa used for each pairwise contrast in the VCV analyses, given the number of taxa without inapplicable states.



Figure 23: Pairwise estimated rate covariance matrices across the five selective regimes, using only taxa with diet data. Covariances scaled to correlations. Selective regimes were mapped onto the tree (22 species with diet data) using a stochastic mapping of the feeding guilds. Tree is pruned to taxa with no inapplicable states for a given character pair. Not all regimes are represented in all contrasts. Question marks represent computationally singular contrasts.

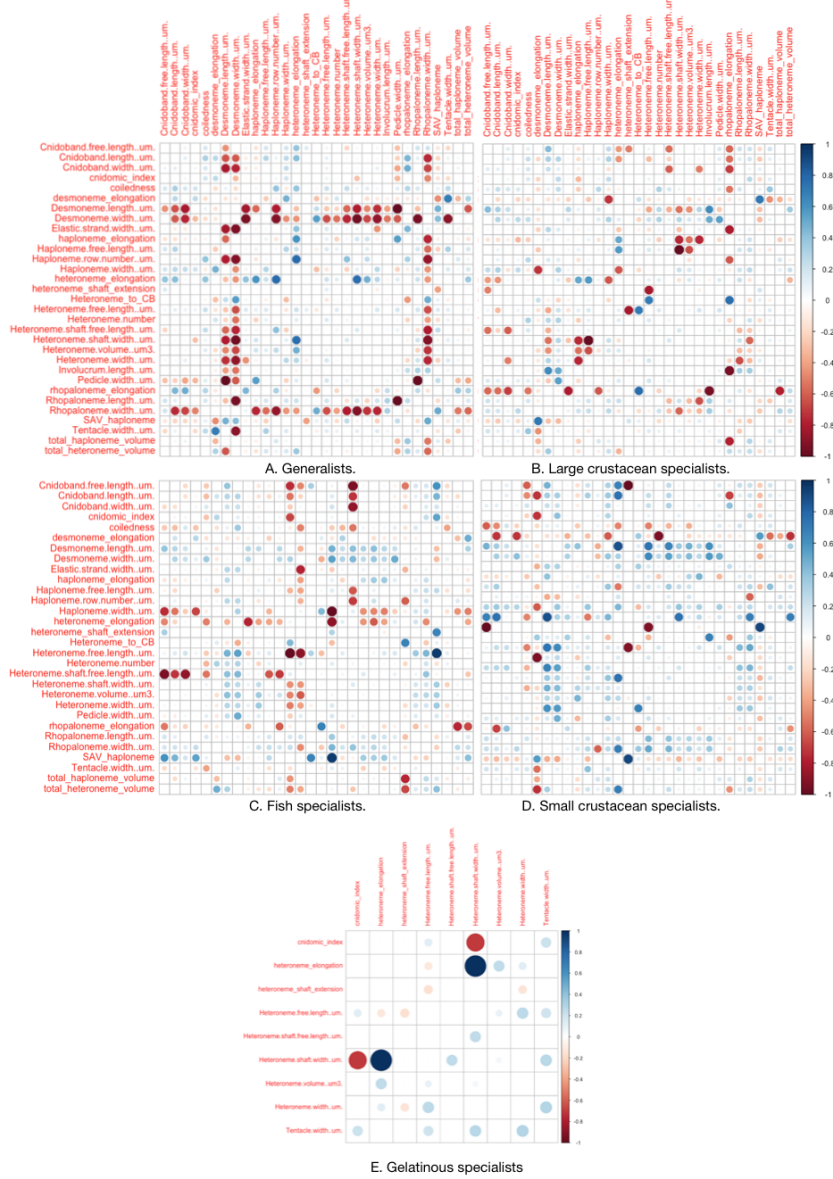


Figure 24: Scaled differences between the regime-specific covariance matrices in @ref{VCV_Regimes} and the whole tree covariance matrix.

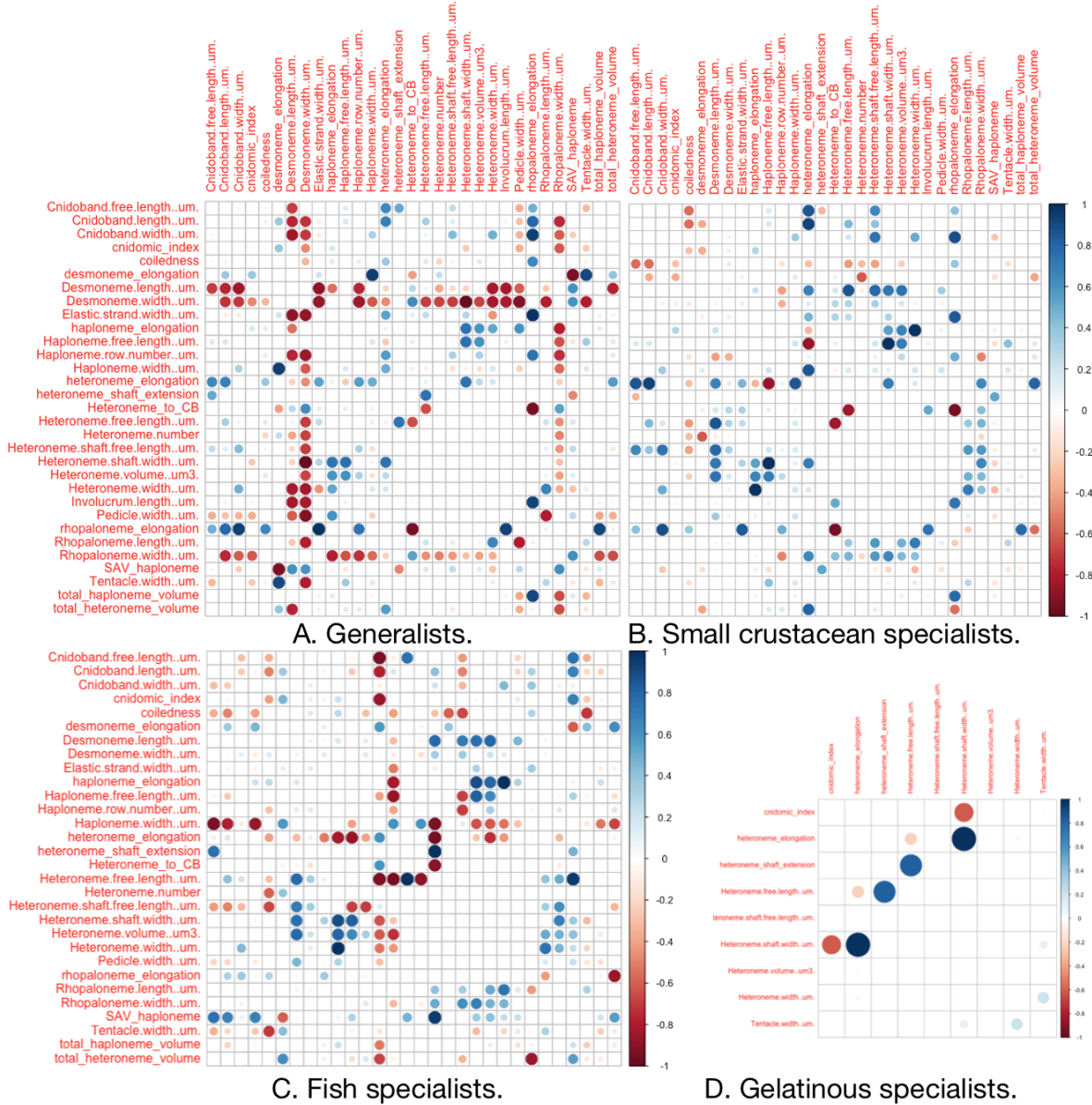


Figure 25: Scaled differences between the regime-specific covariance matrices in @ref{VCV_regimes} and the covariance matrices in their preceding regime, the large-crustacean specialist regime.